Axial Tubules of Rat Ventricular Myocytes Form Multiple Junctions with the Sarcoplasmic Reticulum

Parisa Asghari,[†] Meredith Schulson,[†] David R. L. Scriven,[†] Garnet Martens,[‡] and Edwin D. W. Moore[†*]
[†]Department of Cellular and Physiological Sciences, and [‡]BioImaging Facility, Department of Botany, University of British Columbia, Vancouver, British Columbia, Canada

ABSTRACT Ryanodine receptors (RyRs) are located primarily on the junctional sarcoplasmic reticulum (SR), adjacent to the transverse tubules and on the cell surface near the Z-lines, but some RyRs are on junctional SR adjacent to axial tubules. Neither the size of the axial junctions nor the numbers of RyRs that they contain have been determined. RyRs may also be located on the corbular SR and on the free or network SR. Because determining and quantifying the distribution of RyRs is critical for both understanding and modeling calcium dynamics, we investigated the distribution of RyRs in healthy adult rat ventricular myocytes, using electron microscopy, electron tomography, and immunofluorescence. We found RyRs in only three regions: in couplons on the surface and on transverse tubules, both of which are near the Z-line, and in junctions on most of the axial tubules—axial junctions. The axial junctions averaged 510 nm in length, but they occasionally spanned an entire sarcomere. Numerical analysis showed that they contain as much as 19% of a cell's RyRs. Tomographic analysis confirmed the axial junction's architecture, which is indistinguishable from junctions on transverse tubules or on the surface, and revealed a complexly structured tubule whose lumen was only 26 nm at its narrowest point. RyRs on axial junctions colocalize with $Ca_v1.2$, suggesting that they play a role in excitation-contraction coupling.

INTRODUCTION

The subcellular distribution of ryanodine receptors (RyRs) in a myocyte determines the size, shape, and duration of the whole-cell calcium transient, and it creates microdomains in which the local calcium concentration is far greater than that of the cellular average. If we are to model the calcium transient and to understand local physiological control of calcium-dependent processes, we must know the location of the RyRs, as well as that of the organelles and other molecules to which they are adjacent.

Our current understanding is that most RyRs are located in clusters that are found only in specialized regions of the sarcoplasmic reticulum (SR): the junctional SR (jSR) and the corbular SR (cSR). jSR membranes are positioned 10–15 nm away from clusters of voltage-gated calcium channels, $Ca_v1.2$, that are located either in the sarcolemma or in the transverse-axial tubule system (TATS) (1–3). These closely apposed membrane surfaces and their associated proteins create distinct, unmistakable structures in transmission electron micrographs termed ''junctions'' or ''couplons''. This architecture is essential for normal calcium-induced calcium release and excitation-contraction coupling in the heart (4). Most of the couplons in the TATS are formed with transverse tubules, most properly called ''T-tubules'', that are either at the level of the Z-lines or very near to it and that belong to the transversely oriented regions of the TATS. In addition, some of the couplons are with axial tubules, but the proportion of axial junctions, their size, and the number of RyRs that they contain, have never been determined.

The cSR is a RyR-studded sac, ~100 nm in diameter, containing calsequestrin and storing calcium (5,6). It extends from network SR into the myoplasm, close to the Z-line, but it does not have an adjacent T-tubule or $Ca_v1.2$. This is a prominent feature in cells lacking a TATS, such as avian cells and atrial cells in the mammalian heart, as well as papillary muscle containing T-tubules (7). A quantitative examination of the extent that RyRs occur on the cSR, and on the other organelles to which it is adjacent, has not been reported for ventricular muscle.

In addition to these locations, RyRs have also been reported in mitochondria (8) and in the free (network) SR surrounding the myofibrils opposite the A-band (9). The number of RyRs in mitochondria is unclear, but it has been suggested that RyRs in the free SR may be fairly abundant and might explain the 15–20% of calcium sparks that arise in the A-band, well away from the Z-line and the junctional RyRs (9,10).

Little attention has been paid to the existence of RyRs on axial junctions, even though axial tubules are a well-known feature of adult rat cardiomyocytes (11). A quick examination of rat ventricular myocytes reveals that axial junctions may contain a relatively large proportion of the total number of RyRs, and we hypothesize that most of the axial tubules form junctions with the adjacent SR. To investigate this question, we used a combination of fluorescence microscopy, transmission electron microscopy, and electron tomography.

The results demonstrate that the majority of axial tubules form junctions with the SR and that they share all of the structural features of couplons on the plasmalemma and the

Submitted October 30, 2008, and accepted for publication February 23, 2009.

*Correspondence: edmoore@interchange.ubc.ca

Editor: David A. Eisner.

0006-3495/09/06/4651/10 $2.00

doi: 10.1016/j.bpj.2009.02.058

transversely oriented T-tubules. Axial junctions routinely extend well into the A-band and are occasionally large enough to span an entire sarcomere. Tomographic analysis confirms their structure and reveals an unexpectedly complex morphology of the T-tubule. Axial junctions are surprisingly numerous, and we estimate that they contain as much as 19% of a ventricular myocyte's RyRs. Immunofluorescent labeling shows that RyRs in axial junctions are adjacent to $Ca_v1.2$ and could therefore contribute to excitation-contraction coupling.

METHODS

All chemicals were purchased from Sigma-Aldrich (Oakville, Canada), unless otherwise stated. Animal handling was done in accordance with the guidelines of the Canadian Council on Animal Care.

Tissue processing for electron microscopy

Animals were sacrificed with a peritoneal injection of 2 mL of 1000 units of Hepalean (Organon Canada, Mississauga, Canada) and 2.5 mL of sodium pentobarbital (80 mg/100 g; MTC Pharmaceuticals, Cambridge, Canada). The hearts were perfused for 10 min with physiological saline solution, followed by a fixative containing 4% paraformaldehyde, 2.1% glutaraldehyde, and 4 mM $CaCl_2$ in a 0.1 M cacodylate buffer (pH 7.4; Canemco & Marivac, Lakefield, Canada), for 10 min. The left ventricle was cut into small blocks and the sample immersed in fixative for ~2 h. To speed up the process, blocks were cyclically microwaved (2 min on, 2 min off, 2 min on) in a vacuum using a Pelco 3450 laboratory microwave (Ted Pela Inc., Redding, CA), at power 5 (12). Blocks were rinsed and microwaved twice in 0.1 M cacodylate buffer for 40 s at power 1, then postfixed with 1% OsO_4 solution (EMS, Hatfield, PA) in the same buffer at power 1, then cyclically microwaved twice. This step removed the cytoplasmic matrix from the fractured cells at the cracked surface (13). En-bloc staining of samples was done with 2% aqueous uranyl acetate (Ted Pela), cyclically microwaved twice at power 1, and then rinsed three times with distilled water. They were then dehydrated in increasing concentrations of ethanol (50–100% in steps of 10%; microwave 1 min at each dilution on power 3) and embedded in a mixture of Epon and Spur's resin. From each block, 2-μm-thick sections were cut with a glass or diamond knife mounted on a Leica Ultracut T (Leica Microsystems, Richmond Hill, Canada) and then stained with toluidine-blue. Suitable sections containing surviving myocardial tissues in a longitudinal orientation were selected for study. Ultra-thin sections (80 nm) were cut consecutively from the same block; these were mounted on 0.25% w/v Formvar-coated 200 mesh copper grid (EMS) and double-stained with 2% uranyl acetate for 12 min and Reynold's lead citrate for ~6 min. Sections were investigated using a transmission electron microscope (Hitachi H7600, Hitachi High Technologies America, Schaumburg, IL).

Preparing sections for single-axis tomography

From blocks with regions of well-preserved sarcoplasmic reticula and a tubular system, serial semi-thick (120–130 nm) sections were cut using Leica Ultracut T with a Diatome Ultra 35° diamond knife (Diatome, Hatfield, PA) and collected on 0.5% w/v Formvar carbon-coated slot grids. Poststaining with 2% uranyl acetate for 25 min was followed by Sato's lead citrate for 10–12 min (14). After poststaining, grids were coated with 7.5 nm colloidal gold particles (BBInternational, Cardiff, UK) for 10 min (15) and then Formvar–coated to enhance sample stability in a high-voltage electron beam.

Image acquisition and tomography

Grids were placed in a rotating, high-tilt stage and observed in the Tecnai G^2 Sphera (FEI, Eindhoven, Holland) microscope operating at 200 kV. A suitable longitudinal junction was imaged at 19,000× with serial tilt views from +65° to −65° at 1° intervals, using a camera setting of 1024 × 1024 pixels, resulting in a pixel size of 0.90 nm. The tomograms were generated using TIA software (FEI, Eindhoven, Holland). All tilted images were aligned to a common tilt axis using cross-correlation, and the volume was reconstructed by a real-space back-weighted projection. Tomograms were displayed and analyzed with 3dmod, the graphics component of the IMOD software package (16). The transverse and axial tubules, the sarcoplasmic reticula, the RyRs, and the calsequestrin (CSQ) were modeled manually using procedures detailed in Donohoe et al. (17).

Fluorescence microscopy

Ventricular myocytes were isolated from the hearts of adult-male Wistar rats weighing between 200 and 250 g. Techniques for acquiring myocytes, and for fixation, permeabilization, and immunolabeling, as well as processing, deconvolving, and analyzing images from a wide-field microscope, have been published (18,19). We used an anti-RyR2 monoclonal antibody (Affinity Bioreagents, Golden, CO) and an affinity-purified rabbit polyclonal antibody against the pore-forming subunit of the voltage-gated calcium channel, $Ca_v1.2$ (20). The secondary antibodies were affinity purified and highly cross adsorbed to minimize cross reaction, and were goat anti-mouse conjugated to Alexa 594 and goat anti-rabbit conjugated to Alexa 488 (Invitrogen, Burlington, Canada). Images were acquired using an inverted Zeiss Axio Observer microscope equipped with a Plan Apo 63/1.4 objective and EXFO Xcite illumination (Mississauga, Canada). All filters were from Semrock (Rochester, NY): exciter FF01-494/20-25, dichroic FF506-Di01-25×36, emitter FF01-536/40-25 for Alexa 488 and exciter FF01-575/25-25, dichroic FF593-Di02-25×36, and emitter FF01-624/40-25 for Alexa 594.

RESULTS

The general features common to a junction are shown in Fig. 1 *A*. The variable features are the size of the junction, which can be determined only from serial sections or tomograms, and the architecture; the SR can form a junction with a portion of the T-tubule, as depicted, or it can encircle all (not shown) or most of the T-tubule (Fig. 2 *E*). The architecture changes when the junction is at the cell surface, adopting one of the two configurations shown in the micrographs in Fig. 1, *B* and *C*. Fig. 1 *B* shows a junction straddling a Z-line. The thin SR connects the two halves of the junction, but the electron dense material in the lumen is confined to the region under the RyRs. Seen with equal frequency is a surface junction that is confined to only one side of the Z-line, shown in Fig. 1 *C*. The center-to-center distance between the feet in both internal and surface junctions was the same; 44.3 ± 2.6 nm (mean ± SE; $N = 217$).

We also observed junctions in the interior of the myocyte that are oriented parallel to the cell's longitudinal axis and perpendicular to the Z-line (Fig. 2). Axial junctions have the morphological features of the junctions depicted in Fig. 1, except that they are formed with the axial tubules and they penetrate well into the A-band. The most commonly observed are shown in Fig. 2, *A* and *B*. The former shows an axial tubule that almost spans the sarcomere with a junction that covers only a fraction of its length, whereas the latter shows a shorter tubule with nearly its entire length covered by a junction. Less common are the axial junctions depicted in Fig. 2, *C* and *D*, in which junctions extend almost the entire

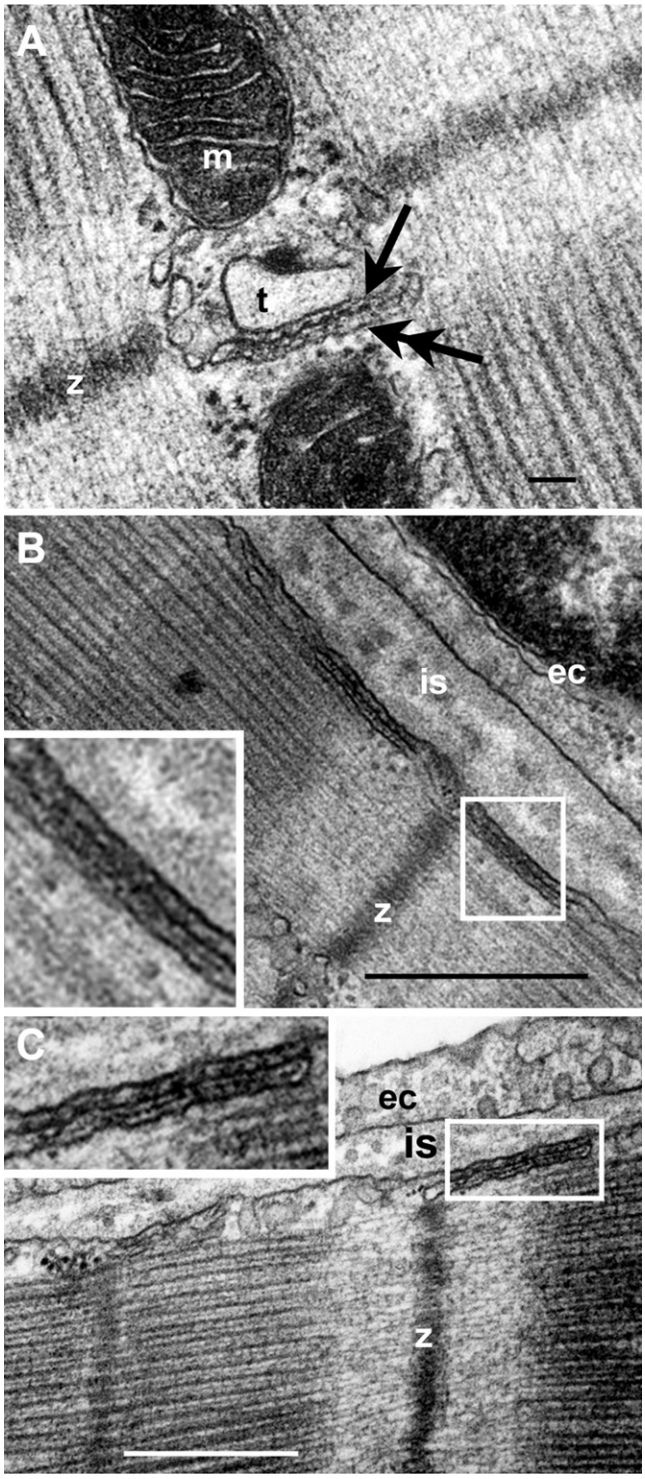

FIGURE 1 Transmission electron micrographs of junctions in the rat ventricle. (*A*) A dyad on the T-tubule: ryanodine receptors (*single arrow*), SR (*double arrow*), mitochondrion (*m*), Z-line (*z*). Scale bar = 100 nm. (*B* and *C*) Surface junctions. Insets of the indicated regions are magnified 2.5×: endothelial cell (*ec*), interstitial space (*is*). Scale bars = 500 nm.

length of the sarcomere. Axial junctions sometimes originate from a junction on the Z-line and can appear as a triad; both of these features are seen in the micrograph in Fig. 2 *D*. Fig. 2, *E* and *F*, shows axial tubules that do not contain junctions. One of these tubules originates from a junction (Fig. 2 *E*) whereas the other does not (Fig. 2 *F*). In 45 micrographs encompassing 804 μm^2, we observed 187 junctions: 148 were junctions with the T-tubule (79%); 39 were with axial tubules (21%). The majority of the axial tubules, 77%, formed junctions with the SR. The center-to-center distance between ryanodine receptors on axial junctions was 40.0 ± 0.88 nm, (mean ± SE; $N = 94$), comparable to that seen in the junctions on the T-tubules and on the surface. The data were obtained from six rats, and no differences were observed between the weight- (200–250 g) and sex- (male) matched animals.

It is clear from Fig. 2 that the axial tubules and the axial junctions have variable lengths, and that the axial junctions do not always occupy the entire length of the axial tubule. To analyze and quantify these relationships, we measured the lengths of the axial tubules and the axial junctions relative to each other, and relative to the sarcomere length. The results are presented in the frequency histograms shown in Fig. 3, all of which are single distributions (Hartigan's dip test for unimodality (21); $p > 0.1$) that are non-Gaussian ($p < 0.01$). We first measured the length of the axial tubules relative to the sarcomere length (Fig. 3 *A*); sarcomere length was 2.04 ± 0.02 μm (mean ± SE; $N = 52$). The frequency histogram presented in Fig. 3 *B* demonstrates that the axial junctions occupy a significant fraction of the axial tubules. Finally, the frequency histogram in Fig. 3 *C* shows that the axial junctions are about one quarter of a sarcomere long, although some are much longer.

In cross section, junctions with axial tubules show the same variability in architecture as do those with T-tubules (Fig. 4). The SR can partially or completely encircle the axial tubule (Fig. 4 *A*), or it can it form a junction with one of the flattened surfaces of the jSR (Fig. 4 *B*). In 19 cross sections, we observed a mean of 8.5 RyRs per longitudinal junction: range 2–24; median = 7.

Atrial cells displayed surface junctions that are indistinguishable from those in the ventricle (Fig. 5 *A*), as well as junctions with transverse axial tubules in those cells that show a rudimentary TATS; an example of an axial junction is shown in Fig. 5 *B*. All atrial cells, regardless of whether or not they possess a rudimentary TATS, display a RyR-studded cSR that is readily apparent on or near the Z-lines; an example is shown in Fig. 5 *C*. The lumen of the SR has electron-dense material, and the magnified inset shows individual RyRs protruding from the membrane into the myoplasm. In contrast, over 200 micrographs of the ventricle failed to find a comparable structure. Instead, we observed sacs of SR protruding into the myoplasm that were clearly devoid of RyRs (Fig. 5 *D*).

To more closely view the association between the axial and transverse tubules, we examined a semi-thick section of 120 nm using tomography (Fig. 6). One of the individual slices of the tomogram is displayed in Fig. 6 *A*, in which the membranes of the transverse and axial tubules, the SR, the electron dense material within the SR, and the RyRs are

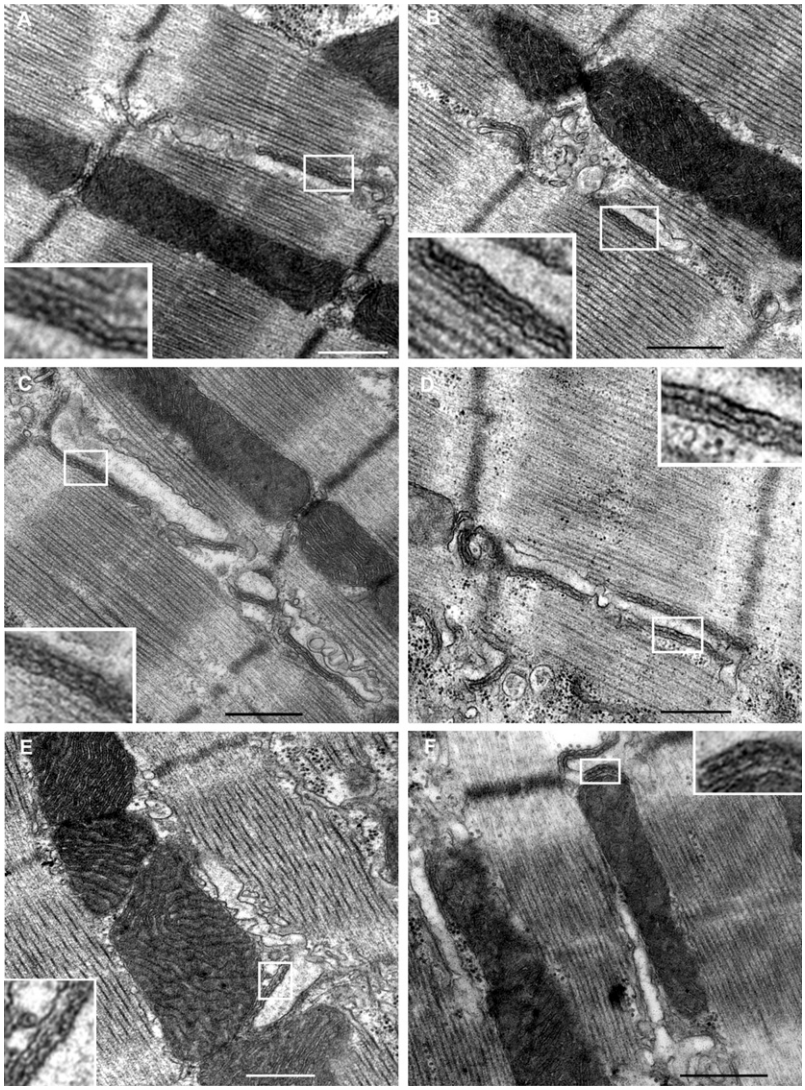

FIGURE 2 Longitudinal sections of axial tubules and their junctions. Insets of the indicated regions are magnified 2.5×. (*A* and *B*) Axial junctions that are a fraction of a sarcomere long. (*C* and *D*) Axial junctions that are a sarcomere in length. (*E* and *F*) Axial tubules without junctions. Scale bars = 500 nm.

clearly visible and have been outlined in different colors (Fig. 6 *B*). The outlines from all 96 planes form a complete 3D model of the data (Fig. 6 *C*), which can be seen in Movie S1 in the Supporting Material. A single row of the ryanodine receptors was clearly visible, and these, along with the SR, are displayed in Fig. 6 *D*.

The axial tubule and jSR have relatively simple morphological features, unlike those features in the transverse tubule, in which multiple and interconnected branches are difficult to visualize. To demonstrate the structure of the tubules, we show two planes from the tomogram, 72.8 nm apart, in Fig. 7, *A* and *C*. Individual sections of the transverse and axial tubules are outlined in Fig. 7, *B* and *D*, and, for clarity and ease of reference, the different parts of the tubules are numbered 1 through 8. The same numbering system was applied to the 3D model (Fig. 7 *E*), which was rotated about the Y and/or Z axes to produce the images in Figs. 7, *F* and *G*. Over the course of 8.4 nm, the axial tubule widened dramatically from ~20 nm (labeled No. 1) to ~180 nm (labeled No. 8). As demonstrated in Fig. 6 *C*, the change in morphological features of the axial tubule was unrelated to the presence of the junction. Tubule 2 is connected to the axial tubule at the point indicated by the arrow in Fig. 7 *E*. Tubule 3 is connected to tubule 4 and to the axial tubule, as shown in Fig. 7, *B*, *E*, and *G*. Transverse tubules numbered 4, 5, 6, and 7 connect at the point indicated by the asterisk in Fig. 7, *F* and *G*; at this point the tubule is an oval 14 nm wide (Fig. 7 *F*) and 115 nm long (Fig. 7 *G*). These four tubules converge and twist, forming an 'X' whose bottom half is rotated ~90 degrees. This can also be seen in Fig. 7, *B* and *D*, in which a line drawn between the center of tubules 4 and 5 in Fig. 7 *B* would be roughly perpendicular to a line drawn between the centers of tubules 6 and 7 in Fig. 7 *D*. Tubule 6 has the smallest diameter and is only 26 nm wide at its narrowest point.

Lastly, we used dual-label immunofluorescence to determine if axial RyRs are adjacent to $Ca_v1.2$ (18,19). A single plane extracted from the 3D image of a cell labeled with antibodies specific for RyRs (*red*) and for the pore-forming

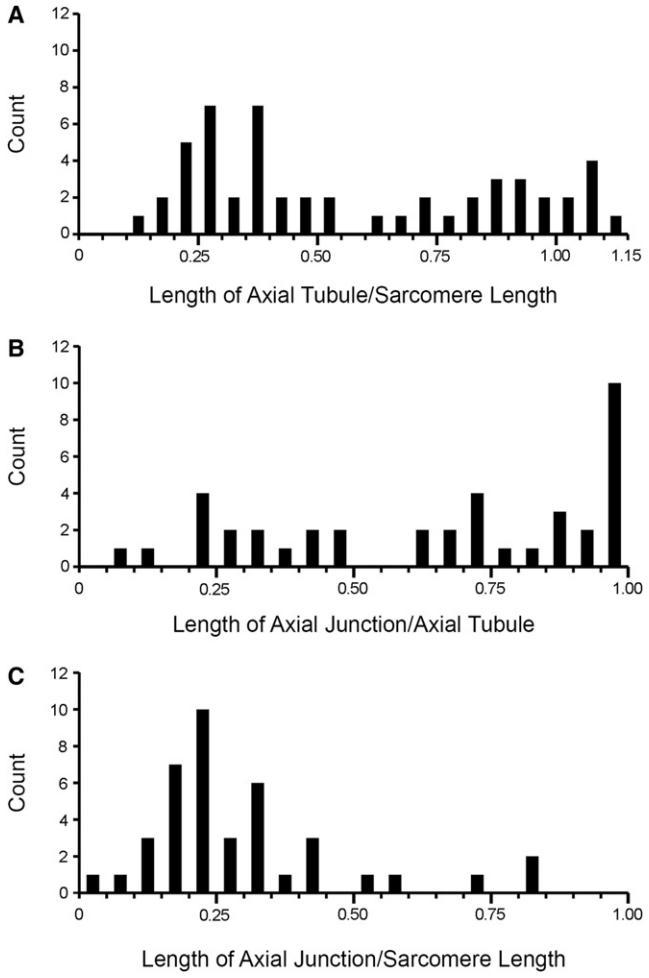

FIGURE 3 Frequency histograms. All bins are one twentieth of a sarcomere long. (*A*) The length of each axial tubule expressed as a fraction of the length of the sarcomere. $N = 52$. Mean = 0.56, median = 0.44, mode = 0.26, SD = 0.31. (*B*) The length of each axial junction expressed as a fraction of the length of its axial tubule. $N = 40$. Mean = 0.66, median = 0.73, mode = 1.00, SD = 0.30. (*C*) The length of each axial junction expressed as a fraction of the length of the sarcomere. $N = 40$. Mean = 0.30, median = 0.24, mode = 0.19, SD = 0.18.

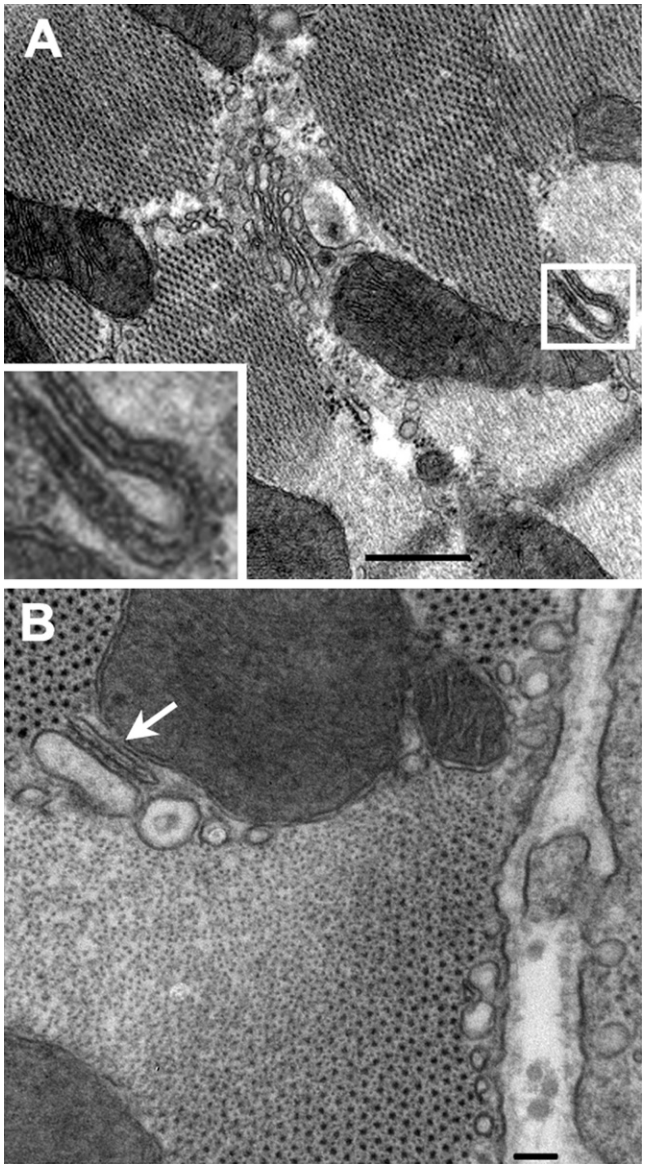

FIGURE 4 Cross sections of axial tubules and their junctions. (*A*) The axial tubule is nearly encircled by the junction. The inset is a 2.5× magnification of the indicated region; the scale bar is 500 nm. (*B*) One surface of the axial tubule forms a junction with the adjacent SR (*arrow*). Scale bar = 100 nm.

α subunit of $Ca_v1.2$ (*green*) is displayed in Fig. 8 *A* (*i*) (colocalized voxels are white). As expected, both proteins are distributed along the Z-lines, a segment of which is highlighted and magnified in Fig. 8 *A* (*ii*). Some of the fluorescence is oriented perpendicular to the Z-lines, on axial junctions. We isolated a total of 70 axial and 70 transverse segments from the images: 10 of each from 7 cells isolated from 4 rats. Two of the axial junctions isolated from the cell in this image are highlighted, and single-image planes are displayed in the insets. Fig. 8 *A* (*iii*) shows a junction extending almost the entire distance between adjacent Z-lines, whereas Fig. 8 *A* (*iv*) shows a smaller junction that extends only part-way into the sarcomere.

The length of the axial junctions, expressed as a fraction of the sarcomere length, was described by a single distribution (Hartigan's dip test, $p > 0.1$) that was non-Gaussian ($p < 0.001$) (Fig. 8 *B*). Although comparable to that measured using transmission electron microscopy, the mean length measured by fluorescence was significantly larger (Mann-Whitney U test, $p < 0.004$), which is not surprising given the different resolving powers of the two techniques.

A notable difference between the transverse and axial junctions displayed in Fig. 8 *A* is the presence of RyRs on the former that have no adjacent $Ca_v1.2$; these are the extradyadic RyRs (Fig. 8 *A*, *ii*; *arrow*). This visual difference is also apparent in the numerical analyses (Fig. 8 *C*). The results show that $Ca_v1.2$ is colocalized with RyRs (*black bars*) to a greater extent than that shown by RyRs with $Ca_v1.2$ (*gray*

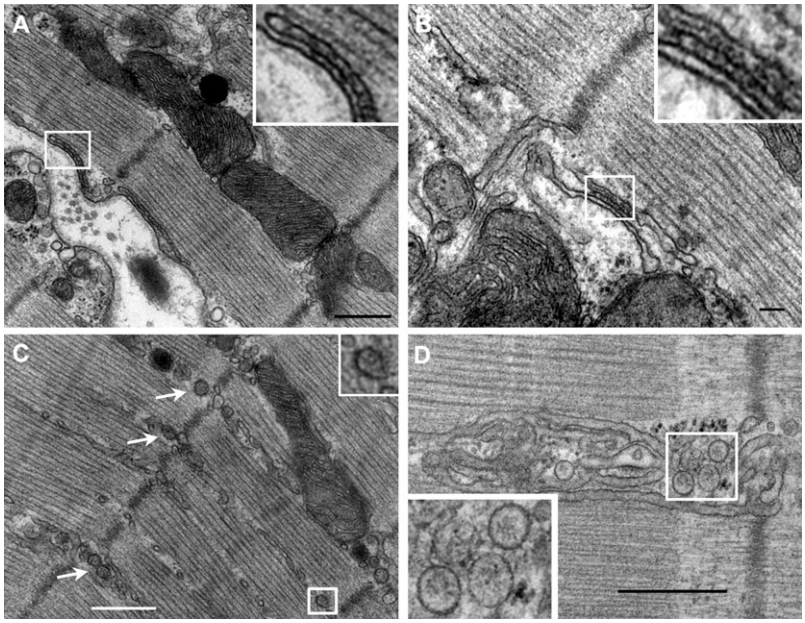

FIGURE 5 Atrial RyRs and Corbular SR. (*A*) Rat atrium, inset is a 3× magnification of the highlighted surface junction. Scale bar is 500 nm. (*B*) Rat atrium, inset is a 3× magnification of the highlighted axial junction. Scale bar is 100 nm. (*C*) Rat atrium. Arrows point to examples of corbular SR. The inset is a 2.5× magnification of the indicated region. (*D*) Rat ventricle. The sacs of SR are devoid of RyRs. The inset is a 2× magnification of the indicated region. Scale bars are 500 nm.

bars; $p < 0.001$) on both axial and transverse junctions, which is in agreement with previous observations (19,22,23). But, there is a significantly greater amount of colocalization of RyRs with $Ca_v1.2$ in the axial segments relative to the transverse segments ($p < 0.001$), because of the lack of extradyadic RyRs.

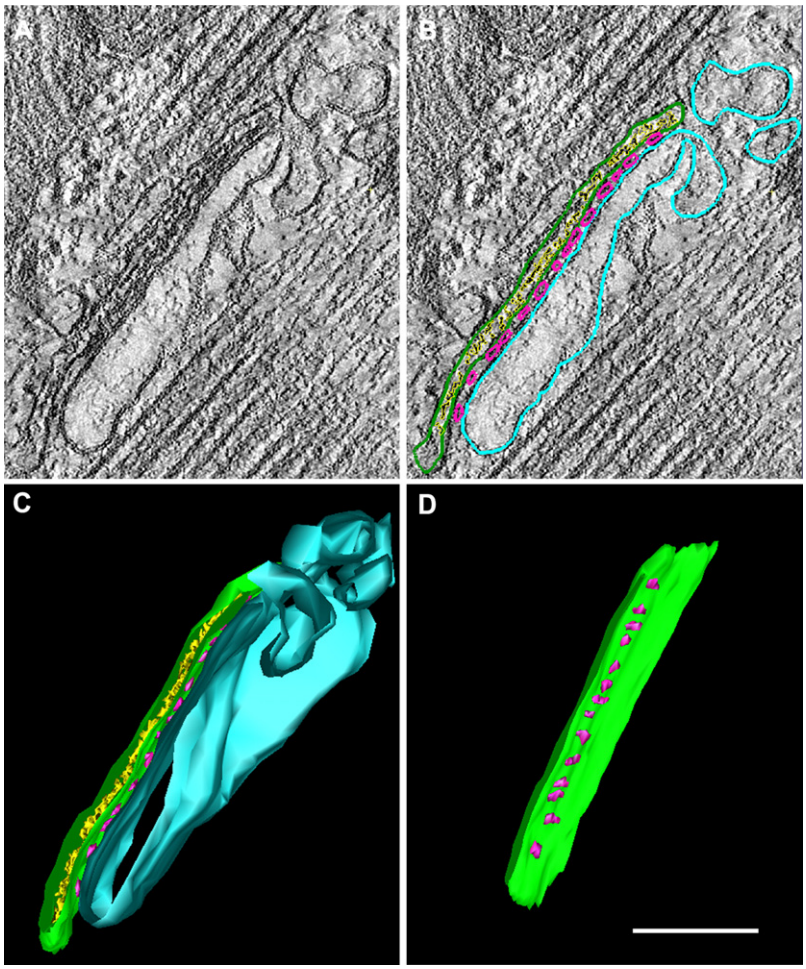

FIGURE 6 Tomography of a single longitudinal junction. Scale bar = 100 nm. (*A*) One plane of the reconstructed tomogram. (*B*) Tracings of the relevant structures from *A*: SR (*green*), individual RyRs (*red*), CSQ (*yellow*), transverse and axial tubules (*blue*). (*C*) The drawings from each of the planes form the 3D model. (*D*) The SR and RyRs have been isolated and rotated 70° about the Y-axis.

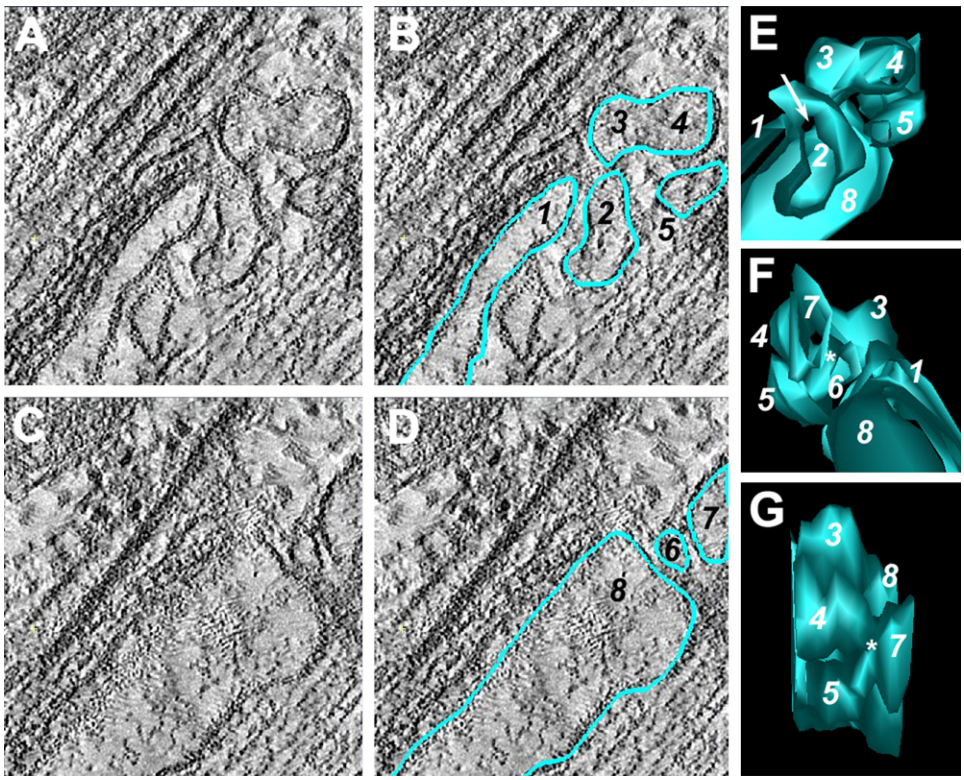

FIGURE 7 Tomography of a single longitudinal junction and the transverse tubule to which it is connected. (*A* and *C*) Planes 14 and 66 of the tomogram respectively. (*B* and *D*) *A* and *C* with the tubules numbered and highlighted in blue. Tubules 3, 4, 5, 6, and 7 are transverse tubules; tubules 1and 8 are axial tubules. 3D rendering of the numbered tubules. (*E*) Orientation is the same as in A–D. Arrow points to connection between tubules 2 and 8. (*F*) E rotated 180 degrees about the Y-axis. The asterisk marks the connection between tubules 6 and 7. (*G*) E rotated −90 degrees about the Y-axis, then −45 degrees about the *X* axis. The asterisk marks the connection between tubules 4, 5, and 7. Tubule 6 is behind tubule 7 and not visible in this orientation.

DISCUSSION

We have examined the distribution of RyRs in adult rat ventricular myocytes. Our primary method was transmission electron microscopy, because RyRs have a characteristic and unmistakable profile in well-preserved and stained sections and because TEM provides direct visualization of the compartment in which the RyRs are located.

The baseline for our measurements was established by examining junctions with T-tubules at the Z-line and junctions with the surface (Fig. 1). These images displayed the expected components in the appropriate spatial configuration. First, the membranes of the sarcolemma and the SR were only ~10–15 nm apart. Second, the lumen of the SR was narrow and contained electron dense material that is thought to be largely calsequestrin. Third, the electron dense ryanodine receptors, or feet, were clearly seen on the SR membrane, spaced at regular intervals extending toward the T-tubule. The variable features were the size of the junction, which can only be determined from serial sections or tomograms, and the architecture; the SR formed a junction with a portion of the T-tubule (Fig. 1 *A*), or it could encircle most or all of the T-tubule (Figs. 2, *E* and *F*, and 5 *A*. All of the axial junctions displayed characteristics identical to those listed for junctions on T-tubules and on the surface (Figs. 2, *A–D*, 4, and 6).

The arrangement of individual RyRs in a native membrane is thought to be that of a regular lattice, with center-to-center distances between individual RyRs of 31.5 nm, or 44.5 nm on the diagonal (24). The distance we measured between RyRs in junctions with the T-tubule (44.3 ± 2.4 nm) and on axial junctions (40.0 ± 0.88 nm) is within this range. On the surface, we observed a roughly equal proportion of junctions that were doublets and singles. Comparable results have been seen in immunofluorescence images in which RyRs on the surface were distributed in doublets on either side of the Z-line (25).

We did not find cSR in ventricular myocytes, although it was readily visible in virtually all of the micrographs acquired from the atria, as expected (6,26). The discrepancy between our findings and those reported in the literature likely stem from the different tissues that were examined: ventricular versus papillary myocytes. The cSR in rat papillary muscle has RyRs (7), as well as CSQ (5,6) and the ability to store calcium (5). If rat ventricular myocytes have cSR, it is very rare. These results indicate that there are structural differences between papillary and ventricular muscles that argue against using the former as a stand-in for the latter.

We searched extensively for RyRs in rat ventricular myocytes and throughout the SR, but we were able to find them in only three locations: junctions with T-tubules on the Z-line, junctions on the surface that may or may not straddle the Z-line, and axial junctions running perpendicular to the Z-line.

Axial tubules were readily visible, and most of the profiles seen in sections, 75%, formed an axial junction with the adjacent SR. It is likely that the remaining 25% also formed junctions that were simply outside of the section and not visible.

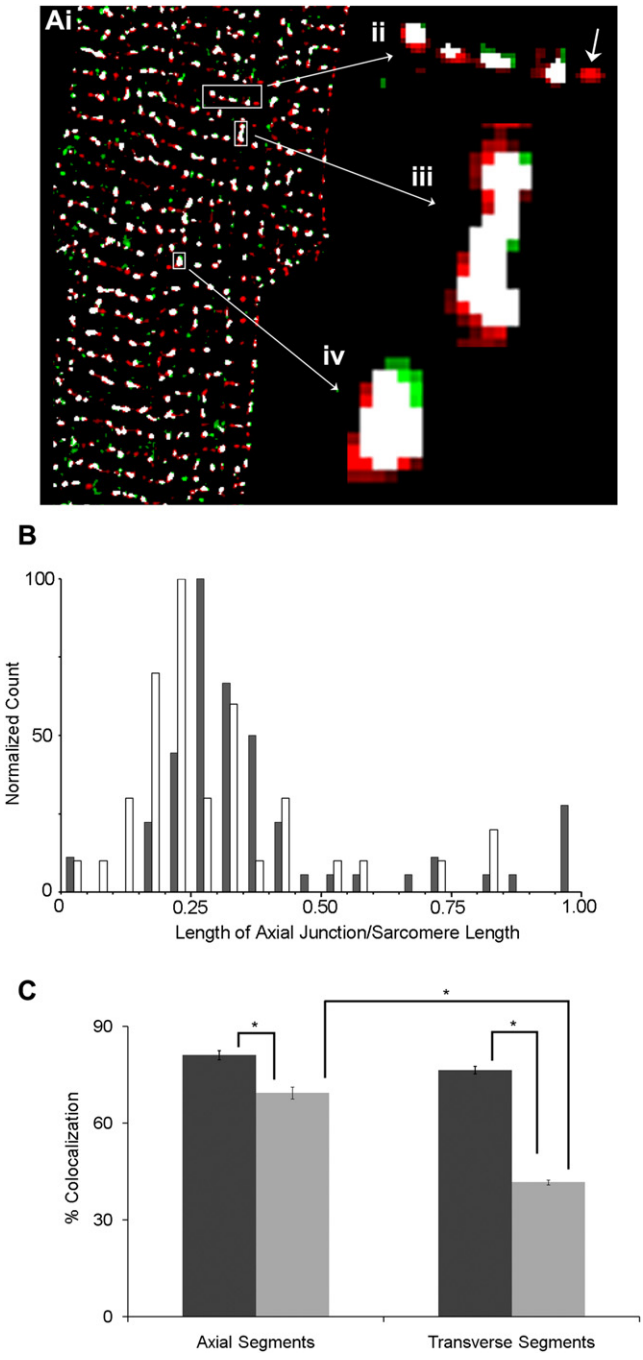

FIGURE 8 (*A*) Rat ventricular myocyte labeled for RyRs (*red*), Cav1.2 (*green*). Colocalized voxels are white. (*i*) A single plane of the data set (278 pixels × 406 pixels × 61 planes), scale bar = 5 μm. (*ii*) 4× magnification of the indicated transverse tubule. Image dimensions are 45 pixels × 18 pixels × 4 planes. (*iii* and *iv*) 10× magnifications of the indicated axial tubules. Image dimensions are 9 pixels × 18 pixels × 3 planes and 9 pixels × 12 pixels × 3 planes, respectively. (*B*) Comparison of the length of the axial junctions measured by fluorescence microscopy (*solid bars*; $N = 70$) and electron microscopy (*open bars*; $N = 40$), normalized to the count in the largest bin. For fluorescence microscopy: mean = 0.39, median = 0.32, mode = 1.0, SD = 0.23. (*C*) The mean colocalization ± SE of RyRs with $Ca_v1.2$ (*gray bars*) and $Ca_v1.2$ with RyRs (*solid bars*). Ten axial tubules and 10 transverse tubules were analyzed from each of seven cells. * indicates a significant difference between the indicated groups, $p < 0.001$.

The length of the axial tubules was variable, but showed a peak at roughly one quarter of a sarcomere in length (mode = 0.26; Fig. 3 *A*). This was true of tubules both with, and without, junctions (Fig. 3, *A* and *C*). The fluorescence images (Fig. 8) also show both short and long stretches of axial RyRs and $Ca_v1.2$, and therefore it is unlikely that short tubules are artifacts caused by sectioning.

Axial tubules have been observed using lipophilic membrane dyes, such as di-8-ANEPPS, in combination with optical microscopic techniques, but this approach only shows the presence of a tubule and cannot reveal the presence of a junction (11,23). Using electron microscopic techniques, RyRs have been observed adjacent to axial tubules (27,28). The significance of our results is in showing that most axial tubules in the rat ventricle have junctions that are quite extensive, sometimes running all the way from one Z-line to the next. They are also frequent, constituting 21% of all the junctions observed in thin sections. Given a median length of 510 nm and 8.5 rows of RyRs, a single axial junction contains, on average, 109 RyRs. Because the T-tubule junctions contain between 120 and 260 RyRs (2,29), we estimate that between 9% and 19% of the cell's complement of RyRs are deployed in axial junctions.

Most RyRs are positioned in jSR opposite clusters of $Ca_v1.2$ in the apposing membrane, either on the surface or in the TATS, but we and other investigators have consistently found that there are RyRs without adjacent $Ca_v1.2$, the extra-dyadic RyR. This is apparent in numerical analyses of immunofluorescence images that always demonstrate a significantly greater colocalization of $Ca_v1.2$ with RyRs than vice versa (19,22,23). An example of an extra-dyadic cluster is shown in the image presented in Fig. 8 *A* (*ii*). In contrast, every axial tubule looked like those displayed in Figs. 8 *A* (*iii* and *iv*): no extra-dyadic RyRs were present. This visual impression was confirmed by the numerical analysis that showed a significantly greater colocalization of RyRs with $Ca_v1.2$ in axial versus transverse tubules (Fig. 8 *C*).

Several lines of indirect evidence suggest that the axial junctions are functional. First, its structural features are indistinguishable from those of the transverse junctions. The axial junctions have both RyRs and CSQ, the distance between the axial tubule and the jSR membrane is only 10–15 nm, and the axial tubule membrane anchors $Ca_v1.2$ opposite RyRs in the jSR. Second, the structural features of the axial junctions in atria are identical to those of the ventricle (Fig. 5 *B*), and these atrial junctions are known to be active participants in excitation-contraction coupling (30). Third, the presence and frequency of RyRs on the axial junctions is sufficient to explain some aspects of calcium dynamics. Up to 20% of a rat ventricular myocyte's spontaneous calcium sparks originate from areas of the sarcomere that are too far from the Z-line to be attributed to T-tubule junctions (9,10). The large and relatively frequent assemblies of RyRs in the axial junctions can easily account for this effect. In addition, it has been difficult to account for the comparable horizontal and

longitudinal conduction velocities of calcium waves if RyRs are only on or near the Z-line (31). Again, our observations suggest that axial junctions could solve that problem. It is therefore reasonable to expect that axial junctions participate in normal excitation-contraction coupling as well as in the production of sparks and the spread of calcium waves.

Electron tomography provided a striking view of the transverse and axial tubules, and their interconnections (Figs. 6 and 7). A video sequence of the reconstructed 3D model (Fig. 6 *C*), is available in the Supporting Material. The most surprising aspects of the data are the tortured path that the tubule follows and the small diameter, 26 nm, of some of the tubules. Both aspects, small diameter and tortuosity, have been noted by others using electron microscopic techniques (27,32), but not those using optical microscopy, possibly because the dyes used to label the tubules cannot diffuse through apertures as small as those we have measured. This would preclude the finer structures from being observed using optical microscopes. Nevertheless, these techniques have revealed a remarkable increase in the number of axial tubules in conjunction with a loss of transverse tubules in failing and chronically ischemic myocytes in the rat (23,33–35).

SUPPORTING MATERIAL

One movie is available at http://www.biophysj.org/biophysj/supplemental/S0006-3495(09)00678-X.

We thank Dr. Clara Franzini-Armstrong for helpful suggestions and for reviewing the manuscript.

We gratefully acknowledge funding from the Canadian Institutes of Health Research (MOP12875) and the Heart and Stroke Foundation of British Columbia & the Yukon to E.D.W.M. The authors would like to thank Dr. W. Catterall for the gift of CNC antibody (National Institutes of Health grant R01 HL085372).

REFERENCES

1. Carl, S. L., K. Felix, A. H. Caswell, N. R. Brandt, W. J. Ball, Jr, et al. 1995. Immunolocalization of sarcolemmal dihydropyridine receptor and sarcoplasmic reticular triadin and ryanodine receptor in rabbit ventricle and atrium. *J. Cell Biol.* 129:672–682.
2. Franzini-Armstrong, C., F. Protasi, and V. Ramesh. 1999. Shape, size, and distribution of Ca(2+) release units and couplons in skeletal and cardiac muscles. *Biophys. J.* 77:1528–1539.
3. Sun, X. H., F. Protasi, M. Takahashi, H. Takeshima, D. G. Ferguson, et al. 1995. Molecular architecture of membranes involved in excitation-contraction coupling of cardiac muscle. *J. Cell Biol.* 129: 659–671.
4. Bers, D. M. 2002. Cardiac excitation-contraction coupling. *Nature.* 415:198–205.
5. Jorgensen, A. O., R. Broderick, A. P. Somlyo, and A. V. Somlyo. 1988. Two structurally distinct calcium storage sites in rat cardiac sarcoplasmic reticulum: an electron microprobe analysis study. *Circ. Res.* 63:1060–1069.
6. Jorgensen, A. O., A. C. Shen, and K. P. Campbell. 1985. Ultrastructural localization of calsequestrin in adult rat atrial and ventricular muscle cells. *J. Cell Biol.* 101:257–268.
7. Jorgensen, A. O., A. C. Shen, W. Arnold, P. S. McPherson, and K. P. Campbell. 1993. The Ca2+-release channel/ryanodine receptor is localized in junctional and corbular sarcoplasmic reticulum in cardiac muscle. *J. Cell Biol.* 120:969–980.
8. Beutner, G., V. K. Sharma, D. R. Giovannucci, D. I. Yule, and S. S. Sheu. 2001. Identification of a ryanodine receptor in rat heart mitochondria. *J. Biol. Chem.* 276:21482–21488.
9. Lukyanenko, V., A. Ziman, A. Lukyanenko, V. Salnikov, and W. J. Lederer. 2007. Functional groups of ryanodine receptors in rat ventricular cells. *J. Physiol.* 583:251–269.
10. Shacklock, P. S., W. G. Wier, and C. W. Balke. 1995. Local Ca2+ transients (Ca2+ sparks) originate at transverse tubules in rat heart cells. *J. Physiol.* 487:601–608.
11. Soeller, C., and M. B. Cannell. 1999. Examination of the transverse tubular system in living cardiac rat myocytes by 2-photon microscopy and digital image-processing techniques. *Circ. Res.* 84:266–275.
12. Galvez, J. J., G. Adamson, M. A. Sanders, and R. T. Giberson. 2006. Microwave tissue processing techniques: their evolution and understanding. *Microsc. Anal.* 20:23–24.
13. Tanaka, K., and A. Mitsushima. 1984. A preparation method for observing intracellular structures by scanning electron microscopy. *J. Microsc.* 133:213–222.
14. Hanaichi, T., T. Sato, T. Iwamoto, J. Malavasi-Yamashiro, M. Hoshino, et al. 1986. A stable lead by modification of Sato's method. *J. Electron Microsc. (Tokyo).* 35:304–306.
15. Penczek, P., M. Radermacher, and J. Frank. 1992. Three-dimensional reconstruction of single particles embedded in ice. *Ultramicroscopy.* 40:33–53.
16. Kremer, J. R., D. N. Mastronarde, and J. R. McIntosh. 1996. Computer visualization of three-dimensional image data using IMOD. *J. Struct. Biol.* 116:71–76.
17. Donohoe, B. S., S. Mogelsvang, and L. A. Staehelin. 2006. Electron tomography of ER, Golgi and related membrane systems. *Methods.* 39:154–162.
18. Scriven, D. R., A. Klimek, P. Asghari, K. Bellve, and E. D. Moore. 2005. Caveolin-3 is adjacent to a group of extradyadic ryanodine receptors. *Biophys. J.* 89:1893–1901.
19. Scriven, D. R. L., P. Dan, and E. D. W. Moore. 2000. Distribution of proteins implicated in excitation-contraction coupling in rat ventricular myocytes. *Biophys. J.* 79:2682–2691.
20. Hell, J. W., C. T. Yokoyama, S. T. Wong, C. Warner, T. P. Snutch, et al. 1993. Differential phosphorylation of two size forms of the neuronal class C L-type calcium channel α1 subunit. *J. Biol. Chem.* 268:19451–19457.
21. Hartigan, J. A., and P. M. Hartigan. 1985. The dip test of unimodality. *Ann. Statist.* 13:70–84.
22. Mohler, P. J., J. Q. Davis, and V. Bennett. 2005. Ankyrin-B coordinates the Na/K ATPase, Na/Ca exchanger, and InsP3 receptor in a cardiac T-tubule/SR microdomain. *PLoS Biol.* 3:e423.
23. Song, L. S., E. A. Sobie, S. McCulle, W. J. Lederer, C. W. Balke, et al. 2006. Orphaned ryanodine receptors in the failing heart. *Proc. Natl. Acad. Sci. USA.* 103:4305–4310.
24. Yin, C. C., L. G. D'Cruz, and F. A. Lai. 2008. Ryanodine receptor arrays: not just a pretty pattern? *Trends Cell Biol.* 18:149–156.
25. Chen-Izu, Y., S. L. McCulle, C. W. Ward, C. Soeller, B. M. Allen, et al. 2006. Three-dimensional distribution of ryanodine receptor clusters in cardiac myocytes. *Biophys. J.* 91:1–13.
26. Dolber, P. C., and J. R. Sommer. 1984. Corbular sarcoplasmic reticulum of rabbit cardiac muscle. *J. Ultrastruct. Res.* 87:190–196.
27. Tomita, Y., and V. J. Ferrans. 1987. Morphological study of the transverse-axial tubular system (TAxTS) in rat heart using ferrocyanide-osmium method and thick sectioning. *J. Submicrosc. Cytol.* 19:523–535.
28. Zhang, L., C. Franzini-Armstrong, V. Ramesh, and L. R. Jones. 2001. Structural alterations in cardiac calcium release units resulting from overexpression of junctin. *J. Mol. Cell. Cardiol.* 33:233–247.

29. Soeller, C., D. Crossman, R. Gilbert, and M. B. Cannell. 2007. Analysis of ryanodine receptor clusters in rat and human cardiac myocytes. *Proc. Natl. Acad. Sci. USA*. 104:14958–14963.

30. Kirk, M. M., L. T. Izu, Y. Chen-Izu, S. L. McCulle, W. G. Wier, et al. 2003. Role of the transverse-axial tubule system in generating calcium sparks and calcium transients in rat atrial myocytes. *J. Physiol.* 547:441–451.

31. Subramanian, S., S. Viatchenko-Karpinski, V. Lukyanenko, S. Gyorke, and T. F. Wiesner. 2001. Underlying mechanisms of symmetric calcium wave propagation in rat ventricular myocytes. *Biophys. J.* 80:1–11.

32. Sommer, J. R., and R. A. Waugh. 1976. The ultrastructure of the mammalian cardiac muscle cell–with special emphasis on the tubular membrane systems. A review. *Am. J. Pathol.* 82:192–232.

33. Bito, V., F. R. Heinzel, L. Biesmans, G. Antoons, and K. R. Sipido. 2008. Crosstalk between L-type Ca2+ channels and the sarcoplasmic reticulum: alterations during cardiac remodelling. *Cardiovasc. Res.* 77:315–324.

34. He, J., M. W. Conklin, J. D. Foell, M. R. Wolff, R. A. Haworth, et al. 2001. Reduction in density of transverse tubules and L-type Ca(2+) channels in canine tachycardia-induced heart failure. *Cardiovasc. Res.* 49:298–307.

35. Heinzel, F. R., V. Bito, L. Biesmans, M. Wu, E. Detre, et al. 2008. Remodeling of T-tubules and reduced synchrony of Ca2+ release in myocytes from chronically ischemic myocardium. *Circ. Res.* 102: 338–346.